

# Ionic Hydrogel for Efficient and Scalable Moisture-Electric Generation

Su Yang, Xiaoming Tao,\* Wei Chen, Jianfeng Mao, Heng Luo, Shuping Lin, Lisha Zhang, and Jianhua Hao

The progress of spontaneous energy generation from ubiquitous moisture is hindered the low output current and intermittent operating voltage of the moisture-electric generators. Herein a novel and efficient ionic hydrogel moisture-electric generator (IHMEG) is developed by rational combination of poly(vinyl alcohol), phytic acid, and glycerol-water binary solvent. Thanks to the synergistic effect of notable moisture-absorption capability and fast ion transport capability in the ionic hydrogel network, a single IHMEG unit of 0.25 cm<sup>2</sup> can continuously generate direct-current electricity with a constant open-circuit voltage of ≈0.8 V for over 1000 h, a high short-current density of 0.24 mA cm<sup>-2</sup>, and power density of up to 35 μW cm<sup>-2</sup>. Of great importance is that large-scale integration of IHMEG units can be readily accomplished to offer a device with voltage up to 210 V, capable of directly driving numerous commercial electronics, including electronic ink screen, metal electrodeposition setup, and light-emitting-diode arrays. Such prominent performance is mainly attributed to the enhanced moisture-liberated proton diffusion proved by experimental observation and theoretical analysis. The ionic hydrogel with high cost-efficiency, easy-to-scaleup fabrication, and high power-output opens a brand-new perspective to develop a green, versatile, and efficient power source for Internet-of-Things and wearable electronics.


## 1. Introduction

Harvesting energy from environment and human has been regarded as a versatile strategy to satisfy increased electric

S. Yang, X. Tao, W. Chen, H. Luo, S. Lin, L. Zhang  
Research Institute for Intelligent Wearable Systems  
The Hong Kong Polytechnic University  
Hong Kong 999077, China  
E-mail: tctaoxm@polyu.edu.hk

S. Yang, X. Tao, W. Chen, H. Luo, S. Lin, L. Zhang  
Institute of Textiles and Clothing  
The Hong Kong Polytechnic University  
Hong Kong 999077, China

J. Mao, J. Hao  
Department of Applied Physics  
The Hong Kong Polytechnic University  
Hong Kong 999077, China

 The ORCID identification number(s) for the author(s) of this article can be found under <https://doi.org/10.1002/adma.202200693>.

© 2022 The Authors. Advanced Materials published by Wiley-VCH GmbH. This is an open access article under the terms of the Creative Commons Attribution License, which permits use, distribution and reproduction in any medium, provided the original work is properly cited.

DOI: 10.1002/adma.202200693

energy demands in widespread applications like Internet of Things (IoT), wearable systems, smart city, etc.<sup>[1–3]</sup> Thermo-electrochemical cell,<sup>[4]</sup> ionic thermoelectric generator,<sup>[5,6]</sup> and moisture-electric generators (MEGs) based on ion migration are booming rapidly. Thermo-electrochemical cells and ionic thermoelectric generator converts low-grade heat into electricity through temperature-dependent redox reactions or ion diffusion. Eminently, MEGs stand out by virtue of inexhaustibility, versatile operational conditions, sustainability, and portability.<sup>[7–11]</sup> In principle, MEGs convert considerable chemical potential energy released by gas-liquid moisture migration in air into useful electric power by constructing oxygen gradient conformation in graphene oxide or water gradient in homogenous polymer films and proteins.<sup>[1,12,13]</sup> Many methods have been attempted to improve their output performance, including asymmetrical structure,<sup>[14,15]</sup> chemical modification,<sup>[16,17]</sup> interface mediation,<sup>[18]</sup> heterogeneous system,<sup>[9]</sup> sunlight-coordinated moisture-electricity,<sup>[19]</sup> and new materials.<sup>[20,21]</sup> Since 2015, Qu et al. has pioneered the work from graphene-based MEGs<sup>[22,23]</sup> with instantaneous output signal, followed by polymer-based MEGs with continuous power generation.<sup>[13,24–26]</sup> Up to now, most of MEGs still suffer from an intermittent mode output signals or an inferior current density in the range of nano-amperes in a continuous mode or micro-amperes in an intermittent mode. With regard to normal electronic appliances, flexible and efficient MEGs with an easy scale-up capability are still challenging to meet the threshold requirement in a few to tens of volts.<sup>[27]</sup> Therefore, it is highly desirable to develop direct-circuit (DC), high-performance, stable, and scalable MEGs toward next-generation energy supply.

Ionic hydrogels are cross-linked polymeric networks with great water capturing and fast ion transport capability through the 3D hierarchical pores.<sup>[28]</sup> Owing to their unique interactions with water molecules, hydrogels with hydrophilic polymer chains (a large number of hydrophilic groups) can promote excellent water molecules absorption.<sup>[29]</sup> Besides, the 3D nanostructured hydrogel frameworks and highly tailorable physicochemical properties with substantial dissociable ions enable fast mass and ion transport under the hydration effect.<sup>[30–32]</sup> Moreover, the low material cost, the high flexibility and ease

of manufacturing of hydrogels provide a fascinating platform for construction of electricity generation device. It is well known that high electric generation of MEGs is closely related to enhanced moisture absorption and ion diffusion process.<sup>[13]</sup> These attractive features empower ionic hydrogels to develop high-efficient MEGs. Currently, hydrogels have been mainly used as binders, electrolytes, and electrode materials for the energy storage<sup>[33–35]</sup> as well as for solar desalination and water purification.<sup>[36]</sup> Conceivably, the tailorable physiochemical properties and favorable structure enable hydrogels more attractive to make big strides forward the green and high-efficient power supply for IoT and wearable electronic.

Herein, we have developed a DC output, efficient, flexible, scalable, and all-weather ionic hydrogel moisture-electric generator (IHMEG) from hydrophilic polymeric network of poly(vinyl alcohol) (PVA)-phytic acid (PA) and hygroscopic glycerin medium. On one hand, the combination of hydrophilic PVA-PA network and hygroscopic glycerol enables IHMEG a high-capability of moisture sorption. On the other hand, PA with six esterified phosphoric acids allows the IHMEG to achieve massive proton dissociation and migration by sufficient hydration effect. A resultant single IHMEG unit provides a stable DC open-circuit voltage ( $V_{oc}$ ) output of  $\approx 0.8$  V for over 1000 h, and a stable DC current of  $9 \mu\text{A}$  for more than 20 h with a matching external load. Besides, the IHMEG is applicable under a wide range of temperature ( $-24$  to  $60$  °C) and relative humidity (10% to 85% RH). Due to the synergistic effect of enhanced moisture-absorption as well as mass ionic clusters diffusion, an areal power density of  $\approx 35 \mu\text{W cm}^{-2}$  of IHMEG is 500 times of that of the best MEGs based on graphene oxide ( $0.07 \mu\text{W cm}^{-2}$ )<sup>[20]</sup> or 7 times of that of protein fiber ( $5 \mu\text{W cm}^{-2}$ )<sup>[1]</sup> in a DC work mode. More importantly, the IHMEG devices demonstrate notable scale-up capability to offer

a  $V_{oc}$  of 210 V in series and a short-circuit current ( $I_{sc}$ ) of 7 mA in parallel, which are sufficient to drive numerous commercial electronics directly, including calculators, electronic watches, a dynamic electronic ink screen, and nickel electrodeposition setup and even light-emitting-diode arrays. With an in-depth analysis by 2D Fourier-transform infrared spectroscopy (2D-FTIR) and micro-Raman spectra, moisture ingress and ionic diffusion process in the hydrogels, as well as the underlying mechanism of IHMEG have been discussed thoroughly. This work opens a brand-new field for the hydrogel as a green and efficient power source for self-powered IoT and wearable electronics.

## 2. Results and Discussion

### 2.1. Fabrication and Structure of IHMEG

A homogeneous hydrogel is constructed by PVA, PA, and binary solvent of glycerol-water. As illustrated in **Figure 1a**, on the skeleton of hydrogel, PA plays the crosslinking role on the gelled hydrogel by reacting with the hydroxyl groups on PVA chains.<sup>[37]</sup> This hydrogel can spontaneously adsorb water molecules from moist air because of its great hydrophilic nature. The abundant micro- or nanopores of dehydrated hydrogel are well observed, providing large number of diffusion paths for ions (Figure S1, Supporting Information). The hydrophilic polymeric network of PVA-PA and hygroscopic glycerin medium enable the hydrogel a great platform to accelerate water absorption and ions migration. One single IHMEG device is connected to the bottom electrode printed on a flexible moisture barrier substrate (like paper, clothing, or poly(ethylene terephthalate) film) as shown in **Figure 1b**. Due to the presence of moisture barrier substrate, the moisture absorption becomes asymmetrical from

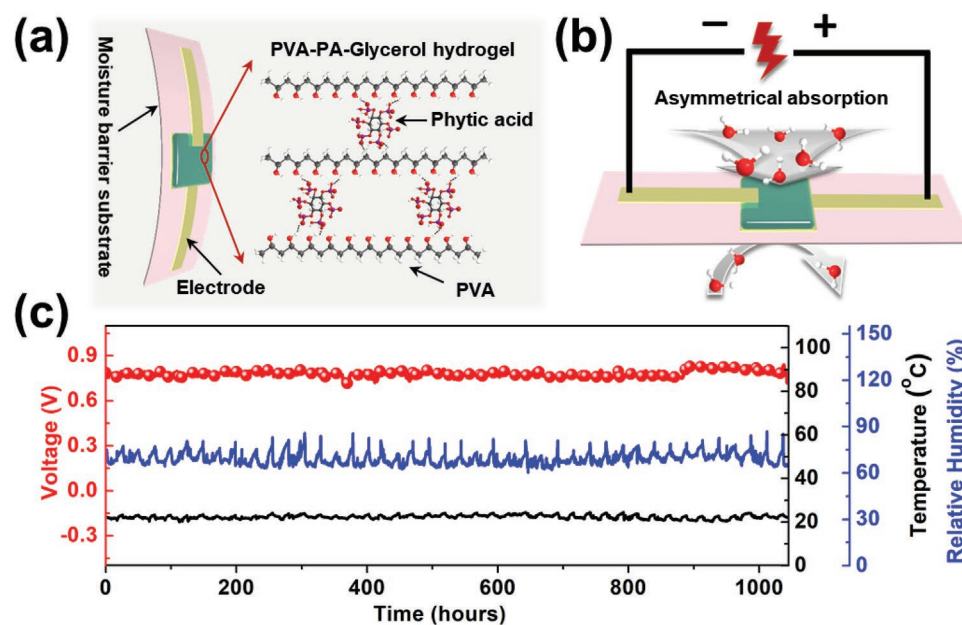


**Figure 1.** Schematic and electric output characteristics of IHMEG. a) The structure of one single IHMEG device with asymmetric-moisture penetration layers. The material consists of PA-gelated hydrogel. b) The schematic diagram of the asymmetric moisture stimulus-induced potential in IHMEG. c) The continuous DC  $V_{oc}$  output (red curve) of an IHMEG device over time under open ambient environment. The ambient relative humidity (blue curve) and temperature (black curve) were synchronously recorded.

both sides, automatically forming a water gradient<sup>[12]</sup> or an ion concentration difference with PA dissociation. To prepare IHMEG (PVA-PA-glycerol), PVA powder and PA solution were added into glycerol-water binary solvent and stirred at 95 °C for 2 h. The resulting homogeneous solution was immediately drop-casted on the moisture insulation substrate with prepared electrodes to form flexible and transparent hydrogel. The binary solvent of glycerol-water imparts remarkable anti-freezing and anti-drying feature of IHMEG device.<sup>[38]</sup> A single IHMEG device can deliver a stable DC  $V_{oc}$  of about 0.8 V for more than 1000 h under an open ambient environment with RH fluctuating from 60% to 90% at  $\approx 22$  °C (Figure 1c), reflecting its outstanding working stability. Whereafter, the voltage output drops over 1020 h presumably due to the decreased water gradient. Such a steady DC voltage output of IHMEG, desperately needed for its intended applications, is different from the intermittent output voltage of many carbon-based MEGs.<sup>[22,39–41]</sup>

## 2.2. Electric Output Characteristics of an IHMEG Unit

It is highly desirable to develop a DC mode output of MEG for powering wearable electronics in all-weather conditions. The IHMEG devices were exposed in a wide range of relative humidity from 10% to 85% RH to determine its environmental humidity-dependent characteristics. Before the test, all samples were short-circuit processed to eliminate possible static electricity. Upon connecting with an external testing circuit at different RHs, the IHMEG generates the DC output signals of both  $V_{oc}$  and  $I_{sc}$  at a specific RH. The  $V_{oc}$  was gradually charged to a steady state at each RH (Figure 2a), and of great significance is that a stable  $V_{oc}$  of  $\approx 0.2$  V can be generated even at a very low RH of 10%, demonstrating a strong all-weather work ability. A largest  $V_{oc}$  of  $\approx 0.88$  V is observed at 85% RH. The  $I_{sc}$  also presents DC mode output closely related to environmental humidity (Figure 2b). An exponential rise of the  $I_{sc}$  is shown with a gradual RH increase (Figure 2c). The  $I_{sc}$  increases from 0.08  $\mu$ A at 10% RH to 2  $\mu$ A at 45% RH, further comes up to an average value of 60  $\mu$ A at 85% RH, two orders of magnitude increase in a row. The accelerated current mainly attributes to enhanced moisture absorption and more free ions diffusion at high humidity to improve electric performance of IHMEG device. In addition, this IHMEG, connected with an external resistor, delivers a steady current output of  $\approx 9$   $\mu$ A even for more than 20 h, where the voltage is lowered to 0.5 V (Figure 2d). Even so, it can restore to its original value after self-charging of 5 h, ready for another constant electrical discharge. A repeatable self-charged and consecutive discharge process has been well observed in Figure 2d, further confirming steady power output capability of this IHMEG.

The IHMEG is also applicable under a wide range of temperature. Figure 2e shows that this IHMEG device engenders decent voltage output from  $-24$  to 60 °C at 80% RH. The current value gradually increases to a platform along with the temperature raising. Different from RH influence, forming water gradient in the asymmetrical structure, the temperature mainly plays a role in improving ionic transport rate and then raises the current density at high value. Even at low temperature ( $-24$  °C), due to excellent anti-freezing ability of glycerol, the IHMEG

can still facilitate a small number of proton dissociation and transport with a low current density of about 18  $\mu$ A  $\text{cm}^{-2}$ . Based on this result, Arrhenius equation is employed to analyze the activation energy of the temperature-dependent current density (Figure S2, Supporting Information). The activation energy ( $E_a$ ) calculated from the slope of the Arrhenius plots gives a value of 16.63  $\text{KJ mol}^{-1}$ , which indicates that vehicle type mechanism is the main contribution to the proton conductivity in our IHMEG device and will be discussed in the following.<sup>[42]</sup> The device performance is also influenced by hydrogel thickness, size, and the contents of PA as well as glycerol (Figure S3, Supporting Information). With the thickness increasing from 0.1 to 1.5 mm, the current density raises up to 0.24  $\text{mA cm}^{-2}$  with stable voltage output of about 0.8 V. While the IHMEG with further thickening shows decreased current density due to long ion diffusion path. The highest volume power density is about 5.9  $\text{mW cm}^{-3}$ , which is comparable to that of protein-based MEG.<sup>[43]</sup> Besides, the  $V_{oc}$  maintains the same whereas the  $I_{sc}$  is gradually enhanced with the increase of hydrogel size. Theoretically, the induced current scales linearly with the area of the IHMEG because of ion-based surface charging effect.<sup>[1]</sup> The appropriate content ratio of PA and glycerol shows optimal power output (Figure S3, Supporting Information). In addition, the IHMEG exerts remarkable endurance and stability under mechanical deformation like bending or compression (Figure S4, Supporting Information), which is of great importance in practical applications. With all-weather adaptability and excellent electric-mechanical performance, IHMEG suffices most of the environmental scenarios over a wide range of RH (10% to 85%) and temperatures ( $-24$  to 60 °C), promising a huge potential as green and wearable power source.

To further investigate the electrical output performance of the IHMEG device, the IHMEG device was connected to different external resistors. As shown in Figure 2f, the output voltage increases while the current density decreases when the electric load varies from 10  $\Omega$  to 500  $\text{M}\Omega$ . A maximum power density of 35  $\mu\text{W cm}^{-2}$  was achieved at an optimal resistance of 10  $\text{K}\Omega$  (Figure 2g). A comparison with other reported MEGs in terms of the maximum  $V_{oc}$  and  $I_{sc}$  is illustrated in Figure 2h and Table S1, Supporting Information. Most MEGs reported previously demonstrate intermittent output feature for both voltage and current, which hampers their practical applications indeed (Table S1, Supporting Information). On the other hand, although a few MEGs are capable to work continuously, their highest  $V_{oc}$  is normally below 0.5 V and the  $I_{sc}$  is smaller than 1  $\mu$ A. On the contrast, our IHMEG possesses a high  $V_{oc}$  of 0.88 V, an obviously larger  $I_{sc}$  of 60  $\mu$ A, and a maximum output power of 35  $\mu\text{W cm}^{-2}$ , 500 times of that of the best MEGs based on graphene oxide (0.07  $\mu\text{W cm}^{-2}$ )<sup>[20]</sup> or 7 times of that of protein fiber (5  $\mu\text{W cm}^{-2}$ )<sup>[1]</sup> in a DC work mode with only moisture-enabled electric generation. The outstanding current density mainly benefits from ionic hydrogel network with moisture capturing ability and fast ion transport capability.

## 2.3. Factors Influencing the Performance of IHMEG

The electric output performance of IHMEG is deeply influenced by moisture and its ingredients. From Figure 3a–c, it is clearly

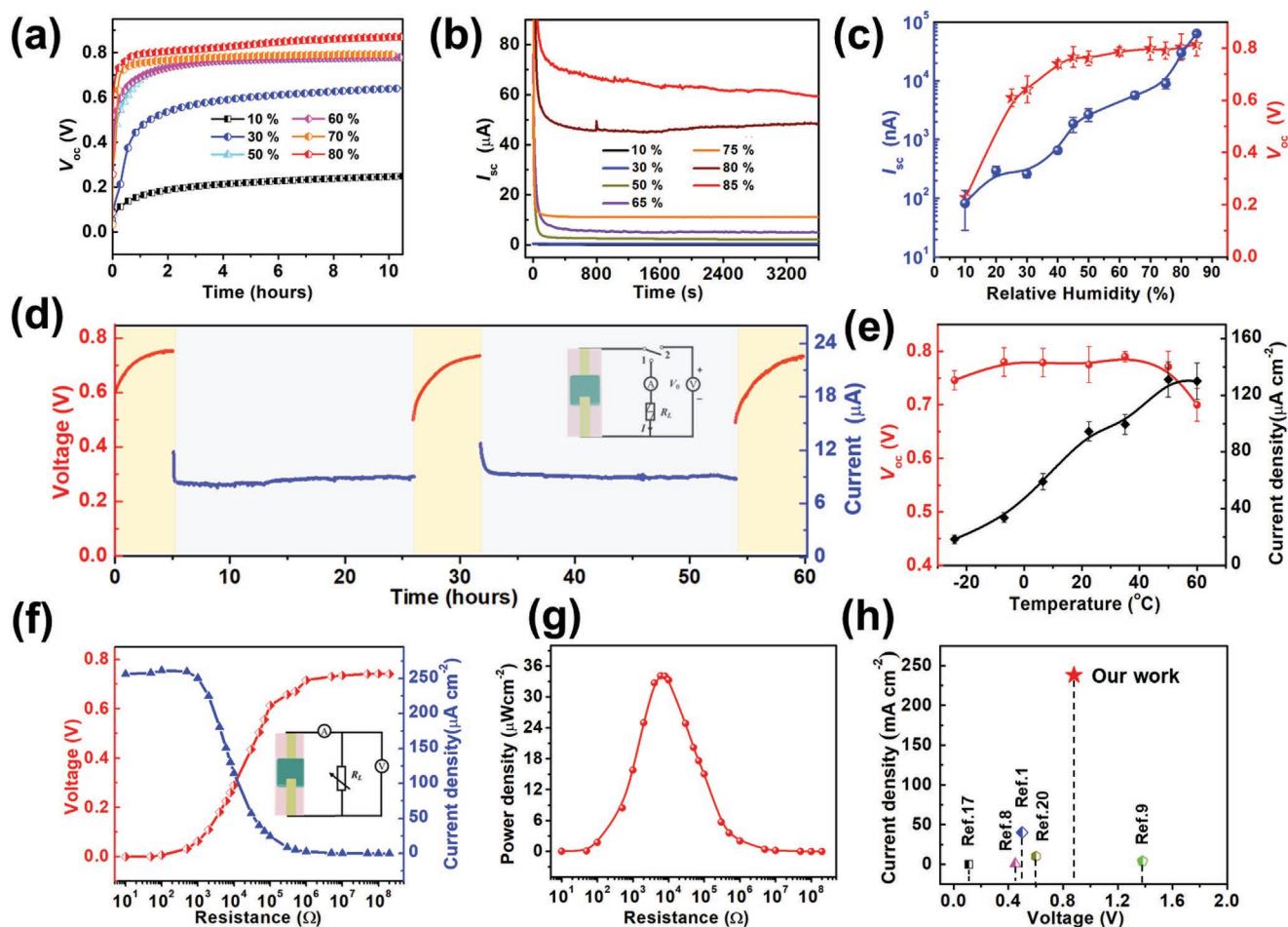


**Figure 2.** a) The curves of  $V_{OC}$  versus time at different RH conditions at room temperature. b) The curves of  $I_{sc}$  versus time at different RH conditions at room temperature. c) The variation of stable  $V_{OC}$  and  $I_{sc}$  versus RH change from 10% to 85%. Data represent the mean  $\pm$  standard deviation ( $n = 4$ ). d) Variations of  $I$  (red) and  $V_{OC}$  (blue) from a working IHMEG device with a switch and an external load (shown in the inset) in the ambient environment (at a relative humidity of about 80%). The device initially had a  $V_{OC}$  of  $\approx 0.76$  V (at times from 0 to 5 h). Connecting to an external resistor ( $R_L = 50$  k $\Omega$ ) yielded a continuous and gradually stabilized DC current of about 9  $\mu$ A for 20 h (blue curve; 5 to 25 h). Then  $R_L$  was disconnected and  $V_{OC}$  was recorded (indicated by the arrow at  $t = 25$  h).  $V_{OC}$  gradually increased to the initial value of 0.76 V (from 25 to 30 h), showing a self-recharging process. Reconnecting to  $R_L$  yielded a repeated continuous powering to the  $R_L$  ( $I$  is  $\approx 9$   $\mu$ A) (blue curve; 30–50 h). Disconnecting the  $R_L$  yielded a second self-recharging process (50–55 h), which brought  $V_{OC}$  back to 0.76 V again. The inset shows the circuit diagram, in which connections to terminals 1 and 2 correspond to  $I$  and  $V_{OC}$  measurements, respectively. e) The  $V_{OC}$  and  $I_{sc}$  in response to different temperature, for a device size of 0.25 cm<sup>2</sup> and thickness of 0.2 mm. Data represent the mean  $\pm$  standard deviation ( $n = 4$ ). f) Electric output of IHMEG device of 0.25 cm<sup>2</sup> size with external resistance varied from 10<sup>1</sup> to 10<sup>8</sup>  $\Omega$  at 85% RH. The inset is the equivalent test circuit diagram. g) The dependence of power density on electrical resistance of the external circuit according to (f). h) The performance comparison of reported moisture-enabled generators with DC voltage output mode by only moisture-enabled electricity.<sup>11,8,9,17,20</sup>

observed that the atmosphere humidity serves as the source of energy input to the IHMEG device. On one hand, the current is highly sensitive to the humidity. When RH increases stepwise from 20% to 80%, the current shows a gradient advance up to 33  $\mu$ A. Furthermore, the current is immediately promoted after relieving the vacuum and then the electric output is drained followed by immediate vacuuming (Figure 3b). On the other side, the IHMEG device generates low voltage output after 2 days' dehydration at 10% RH. Whereafter, the elevated humidity facilitates the gradient elevation of electric output to about 0.8 V (Figure 3c), well consistent with above-mentioned humidity-dependent electric performance (Figure 2c). Besides, due to the presence of the moisture-barrier layer, there exists the asymmetric moisturizing direction for IHMEG impacting the potential

generation. Figure 3d shows that the lower-moisture side of IHMEG device always has a higher potential. When the positive electrode of testing circuit is connected to the bottom electrode with lower humidity (red curve), the induced voltage is positive. Once exchanging the connection, the opposite voltage output (black curve) is presented. Furthermore, when the upper side of the hydrogel is turned over to contact the moisture barrier substrate, the voltage remains unchanged a little (Figure 3e). That means the power generation is dependent on the moisturizing direction. Dynamic asymmetric moisture absorption process in IHMEG occurs spontaneously when exposed to the air, which creates distinct moisture gradient between the top surface and the bottom of the hydrogel. Then the moisture starts to migrate from top to bottom, along with dissociated protons from the

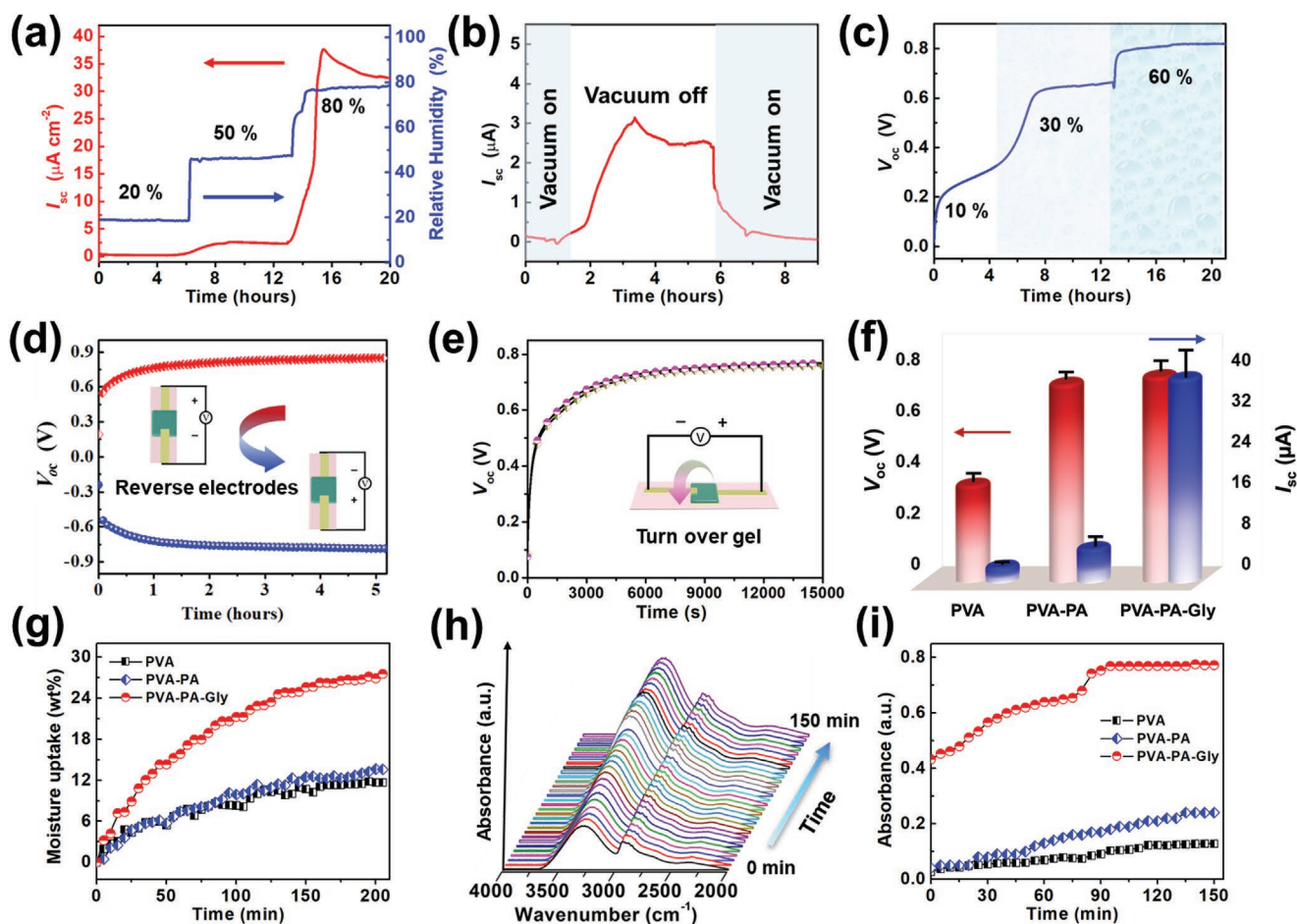


**Figure 3.** Analysis of energy-generation derivation. a) Evolution of  $I_{sc}$  (red) with step-changes of relative humidity (blue) versus time. b) Stepwise current development under vacuum-relief-vacuum environment. c) The  $V_{oc}$ -versus-time plot in response to the step increase in relative humidity. Before test, the IHMEG device was vacuumed and dried for 2 days. d) Polarity test of the IHMEG device. The sign of the induced voltage is reversed after the electrodes of the source-meter are turned over. e) The output voltage of the IHMEG before and after turning over the upper side of hydrogel to the moisture barrier substrate, corresponding to the pink and brown curve, respectively. f) Comparison of  $V_{oc}$  and  $I_{sc}$  made from PVA, PVA-PA, and PVA-PA-glycerol (IHMEG). Data represent the mean  $\pm$  standard deviation ( $n = 4$ ). g) The moisture uptake capability with time after the dried samples are exposed in the atmosphere (60% RH). h) The in situ FTIR spectrum tracking once the samples are exposed in the atmosphere (60% RH) versus time for PVA-PA-glycerol. i) The semi-quantitative analysis of water-absorbing peak (3700–3000  $\text{cm}^{-1}$ ) with time according to Figure S6a–c, Supporting Information.

structure of PA. Due to excellent water-absorbing ability of hydrogel, the IHMEG lowers the RH threshold to initiate ion dissociation and migration. Consequently, higher levels of voltage and current generate. Otherwise, extremely low RH or little moisture difference encumbers ion transport and then results in low voltage and current.

The compositions of IHMEG from ionizable polymeric network of PVA-PA and hygroscopic glycerol medium exert a synergistic effect on elevating the output power. The control sample PVA film delivers a low voltage output of 0.38 V and an extremely low current, which is consistent with previous report.<sup>[13]</sup> Once the PA is added into the matrix, the voltage has a doubling increase as shown in Figure 3f. It is mainly because PA plays as the crosslinking points with the hydroxyl groups on PVA chains. Once exposed in the moisture, the protons dissociate from the PA, while the skeletons of PA still adhere to the PVA chains, then forming an internal electric field and

improving voltage output. More importantly, there appears a significant improvement of current for the IHMEG (PVA-PA-glycerol) with the addition of hygroscopic glycerol medium. Herein glycerol significantly enhances the moisture absorption capability of IHMEG meanwhile forms weaker H-bond interaction within hydrogel (Figure S5, Supporting Information), then facilitating the easier ionization and faster transport of the protons. The improved moisture-uptake capability is further confirmed by weighting and time-resolved FTIR spectroscopy. Figure 3g demonstrates the moisture uptake rate increases very fast first followed by a slower increase process for these three samples. Finally, the whole samples maintain a dynamic equilibrium with water absorption and desorption. Clearly, PVA-PA-glycerol hydrogel exhibits the fastest and maximum water absorption capability. The PVA and PVA-PA show inferior moisture uptake process due to stronger H-bond interactions for PVA and PVA-PA (Figure S5, Supporting Information). In

addition, time-resolved FTIR spectroscopy as a powerful tool was employed to provide insights into the influence of dynamic absorption and diffusion processes of water molecules on the electric-generation performance for the first time (Figure 3h). The peak intensity of O–H stretching absorption peaks at the range of 3700–3000  $\text{cm}^{-1}$  is closely related to water absorption, which has been in situ tracked over time for PVA, PVA-PA, and PVA-PA-glycerol once they are exposed in the atmosphere of 60% RH (Figure S6, Supporting Information). O–H stretching absorption peaks enhance with the moisture absorption, followed by reaching a platform. After normalizing the intensity of absorption peak, the absorption and diffusion curves of the water are compared and illustrated in Figure 3i. Similarly, PVA-PA-glycerol hydrogel demonstrates the highest absorption peak and the strongest ability to adsorb and accommodate more water. It seems that the ionizable polymeric network of PVA-PA can mainly enhance the voltage but not the current. The elevated current density in IHMEG mainly benefits from the high-capability moisture sorption and weaker H-bond interaction of IHMEG hydrogel network, which accelerates ionization of PA and facilitates rapid mass ion migration in IHMEG. Instead, PVA and PVA-PA with inferior water uptake capability and stronger H-bond interactions lead to less water absorption and a rather slow water diffusion process. The corresponding small moisture-water chemical energy conversion is still not enough to dissociate protons within polymeric network of PVA-PA due to the PVA chain entanglement and the physical crosslinking with PA. Consequently, PVA and PVA-PA present small current densities. These results clearly manifest the synergistic effect of ionizable polymeric network of PVA-PA and hygroscopic glycerol on the high power generation of PVA-PA-glycerol hydrogel.

## 2.4. Working Mechanism of IHMEG

Many theoretical models have been proposed to explain electric generation by using various water motions, such as water dragging model,<sup>[44]</sup> water-infiltration model,<sup>[45]</sup> water-evaporation model,<sup>[46,47]</sup> and gradient ion diffusion model. As for the MEGs, herein, moisture absorption enabled proton dissociation and transport have been proposed to account for the power generation of MEGs in previous works.<sup>[1,13]</sup> Noteworthy, this ionic hydrogel based MEG also abides by this principle. In details, two key points should be responsible for the enhanced power output, that is, improved moisture uptake capability and accelerated ion diffusion process. The PVA-PA-glycerol hydrogel has been proved as a great platform to capture mass gaseous moisture, which is further turned into liquid state, meanwhile releasing enough chemical potential energy to enable the ion dissociation of PA (Figure S7, Supporting Information). Furthermore, the weaker hydrogen band within IHMEG hydrogel empowers a rapid ion transport compared to PVA film with stronger hydrogen band. Thus, the IHMEG generates a higher current density and voltage output than control one. On this basis, we further reveal the underlying mechanism from the molecular level to gain deeper insight and more comprehensive understanding of moisture-enabled electric generation phenomenon by hydrogel-based MEG. Herewith, a powerful

technique, 2D-FTIR spectroscopy was further employed to investigate molecular interactions during the water diffusion into IHMEG by deconvoluting highly overlapped bands for the spectral range of 3700–3000  $\text{cm}^{-1}$  (Figure 4a). Synchronous and asynchronous spectra were depicted explicitly in Figure 4a,b.

One strong and positive auto peak in the synchronous spectrum (Figure 4a) indicates that the O–H stretching band of water strengthens with the water diffusion. Asynchronous spectra in Figure 4b shows two negative cross-peaks (3544/3290, 3436/3290  $\text{cm}^{-1}$ ) and one positive cross-peak (3290/3075  $\text{cm}^{-1}$ ) in the upper left side of the main diagonal, indicating that the water stretching band is split into four separate bands located at 3544, 3436, 3209, and 3075  $\text{cm}^{-1}$ . According to the rules by Noda,<sup>[48]</sup> the four bands vary following the total sequential order is 3290  $\rightarrow$  3075  $\rightarrow$  3544, 3436  $\text{cm}^{-1}$ . This result elucidates at least the formation of four different states of water in IHMEG matrix, corresponding to strong bound water (3075  $\text{cm}^{-1}$ ) forming strong hydrogen bonds between each water molecule or with polymer internal network, cluster water (3290  $\text{cm}^{-1}$ ) forming moderate hydrogen bonds with easy-coupled ions, weak bound water (3436  $\text{cm}^{-1}$ ) interacting with hydrophilic groups in polymer matrices, and free water (3544  $\text{cm}^{-1}$ ) approximately without hydrogen bonding with other molecules.<sup>[49]</sup> Hence the water diffusion follows the sequence: cluster water  $\rightarrow$  strong bound water  $\rightarrow$  weak bound water, free water. That means the water diffuses into the IHMEG membrane in the cluster water forms first as illuminated in Figure 4g. The strong bound water moves more slowly with its stronger hydrogen bonds and its larger size,<sup>[50,51]</sup> which are further confined in the cross-linked hydrogel network and form weak-bound water or free water molecularly dispersion within dense nanopores of hydrogel network. The low dissociation constant ( $\text{pKa} \approx 1.5$ ) of the six protons of PA enables their easy dissociation when encountering the sufficient cluster water, then forming protonated water clusters ( $\text{H}_3\text{O}^+$  or  $\text{H}^+(\text{H}_2\text{O})_n$ ).<sup>[37]</sup> As indicated in Figure S2, Supporting Information, the vehicle type mechanism made the main contribution to the high proton conductivity in our IHMEG device.<sup>[42]</sup> In this situation,  $\text{H}_3\text{O}^+$  or  $\text{H}^+(\text{H}_2\text{O})_n$  ionic clusters transport as a vehicle to form a large diffusion current and internal potential (Figure 4g).<sup>[52]</sup> Besides, in situ Raman spectroscopy mapping was employed to track the sorption path of water molecules on hydrogel surface by detecting Raman band ratio O–H bond/C–H bond (Figure 4c). The result shows that a prominent color change is well observed with the time of moisture sorption (Figure S8, Supporting Information). More importantly, the long existence of moisture gradient between two sides is well observed by in situ 2D Raman mapping even after 7 days (Figure S9, Supporting Information). The top surface of hydrogel has obviously captured more water molecules than the bottom surface, which induces a built-in water gradient. These water molecules keep a dynamic absorption-desorption exchange at the interface to provide a sustained energy input.<sup>[1]</sup> Hence, by virtue of enhanced moisture capture and fast ion transport of porous hydrogel network, as well as remained moisture gradient, IHMEG generates a stable electric output. While the PVA film owns strong hydrogen bond, which is so hard to dissociate the ions from the surface meanwhile the strong hydrogen bonds make it difficult to water diffusion, leave alone the ion dissociation and diffusion.

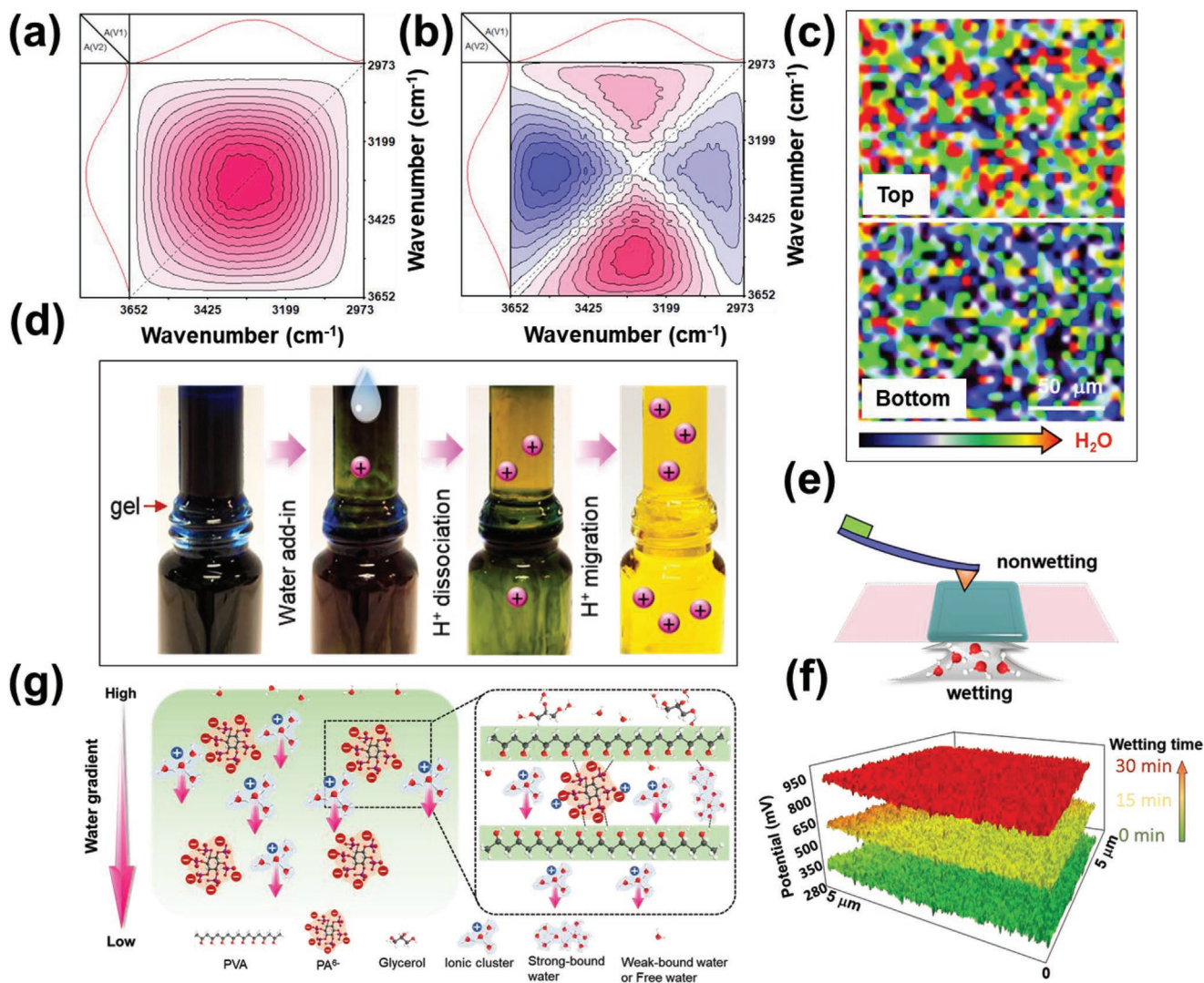


**Figure 4.** The underlying mechanism of IHMEG. 2D-FTIR correlation spectra in the 3700–3000  $\text{cm}^{-1}$  wavenumber region: a) synchronous; b) asynchronous contour maps for IHMEG samples when exposing in the air. The pink area and blue area denote the positive and negative correlation peaks, respectively. c) The water diffusion difference between the top and the bottom surface of hydrogel by 2D Raman mapping after 120 min. d) Photos of the experiment for visualizing the dynamic change of the moisture-induced ionic diffusion process. A piece of the hydrogel is sandwiched between the open ends of two cylindrical containers, the upper tube has two open ends and the bottom one has one open end and one closed end. They are filled with bromophenol blue/isopropanol solution. Water is added into the upper tube through the open end. The color change in the two tubes indicates the dynamic diffusion of dissociated protons with water diffusion. e) Schematic plot of the setup for the Kelvin probe force microscope (KPFM) test and f) the potential change of hydrogel. A piece of hydrogel (250  $\mu\text{m}$  thickness) absorbed moisture from one side and the other side was covered without wetting. The potentials of the two sides are detected by KPFM. The scan range is  $5 \times 5 \mu\text{m}$ . The lower right picture shows the potential increment of the hydrogel after water diffusion from the wetting side to non-wetting side from 15 to 30 min. g) The proposed mechanism of moisture-induced ionic diffusion process.

To further confirm the above mechanism, the water diffusion coupled with ions migration is visually proved by acid indicator (bromophenol blue/isopropanol solution). Bromophenol blue will change color from blue to yellow corresponding to the pH value changing with acid increasing.<sup>[13]</sup> As shown in Figure 4d, when water is added, the bromophenol blue close to the upper surface of the hydrogel membrane first becomes yellow, indicating the free protons being dissociated from the hydrogel. With further water diffusion, the coupled protons migrate from the top to bottom tube until the bromophenol blue/isopropanol solution becomes totally yellow (within 3 min). In clear

contrast, there is little color change of bromophenol blue/isopropanol solution in the control sample PVA (Figure S10, Supporting Information) after 24 h moisturization, corresponding to a low current and voltage output. It well manifests the moisture induced mass ion diffusion is the key to the high electric generation of IHMEG. Furthermore, KPFM was applied to probe the potential change of the hydrogel with wetting for 15 and 30 min. The result shows that the side of hydrogel without wetting becomes more and more positive from  $\approx 300$  to  $\approx 920$  mV because of the water-induced proton diffusion (Figure 4f). In contrast, the potential of wetted side remains

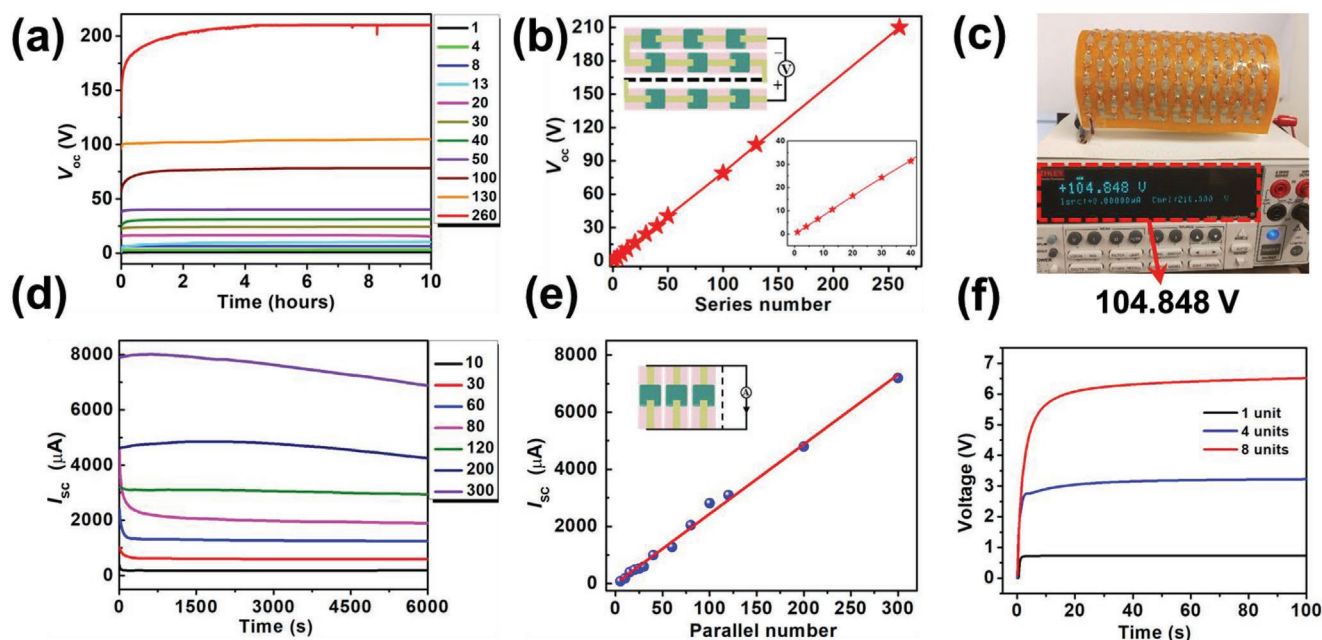


**Figure 5.** Power devices by integration of IHMEG units in serial or parallel packages as a practical DC source for commercial low-power electronics. a) Voltage output of a serial IHMEG units with different series number. The test condition is 65% RH. b) The  $V_{oc}$  related to the serial number of device units. Inset is the equivalent circuit scheme of serial IHMEG units. c) The picture of the voltage output of flexible IHMEG with 130 units in series. d) Current output of a single IHMEG package with different parallel number. e) The  $I_{sc}$  related to the parallel number of device units. Inset is the equivalent circuit of the parallel IHMEG package. f) Voltage–time curve of a commercial capacitor with  $47 \mu\text{F}$  directly charged by a serial IHMEG units with 1, 4, and 8 units.

almost the same (Figure S11, Supporting Information) with the time of water diffusion. Clearly, the water diffusion induced ions migration provokes the increase of potential. Combined with experimental observation and theoretical analysis, it is safe to believe that the directional movement of the protons coupled with fast moisture diffusion accelerates the high-power generation. Clearly, the synergistic effect of strong moisture-absorbing capability within hydrogel network, fast ionic clusters transfer of porous structures, as well as long-standing moisture gradient jointly empower the IHMEG stable power-output performance for a long time.

## 2.5. Scalability of IHMEG Units as a DC Power Source for Applications

To achieve the large-scale integration is a pivotal step toward practical applications of IHMEGs. To this end, the circuits with the bottom electrodes were fabricated on a flexible substrate by a screen-printing method, the PVA-PA-glycerol hydrogel was dropped on the bottom electrodes, followed by placing top electrodes by the end-to-end connection to achieve large-scale series-connected devices. The sizes and numbers of the integrated IHMEG units can be designed according to application requirements of operating voltage and current.

Such versatile, flexible, and light-weight power devices can be scaled up to satisfy practical applications. Figure 5a illustrates the basically linear increment of the  $V_{oc}$  of a serial connected device with the increasing number of IHMEGs. One single IHMEG offers an average voltage of 0.8 V and 100 units of

IHMEGs generate a stable voltage of about 80 V. Furthermore, the 260 IHMEG units connected in series offer an  $V_{oc}$  of about 210 V and stay stable continuously for more than 10 h. A linear relationship is well depicted in Figure 5b, which demonstrates the excellent scaling performance of the IHMEGs. Figure 5c shows that the flexible IHMEG with 130 units in series can generate about a high voltage of  $\approx 105$  V even at a bending state. More interestingly, the IHMEG devices are highly flexible and portable. And they also can be integrated on the flexible poly(ethylene terephthalate) film and clothing (Figure S12, Supporting Information), showing great potential for wearable electronic systems. The parallel integrated IHMEGs also show great linear scale-up performance. As depicted in Figure 5d,e, the total short-circuit current of  $n$ -IHMEG connected in parallel follows a linear relationship of  $n I_{sc}$  with a total voltage of 0.8 V. One single cell produces a continuous  $I_{sc}$  of  $\approx 25 \mu\text{A}$  at 65% RH. A parallelly connected device can reach about 7 mA with 300 IHMEGs at 6000 s. Estimating the power output, the power of parallel-connected IHMEG arrays shows good linear scale-up capability with parallel number and increases up to 1.5 mW for  $1 \times 300$  parallel IHMEG arrays (Figure S13, Supporting Information). Furthermore, DC power source devices can be easily designed and fabricated by connecting IHMEG matrix in serial  $\times$  parallel combinations for practical applications. Moreover, the electricity generated by IHMEGs can be quickly stored in commercial capacitors without the need of extra rectifiers. It is so easy to charge commercial capacitors with capacitance from 47 to 3300  $\mu\text{F}$  in less than 10 min (Figure S13c, Supporting Information). Thus, with serial connections, a power device of multiple IHMEGs can be selected



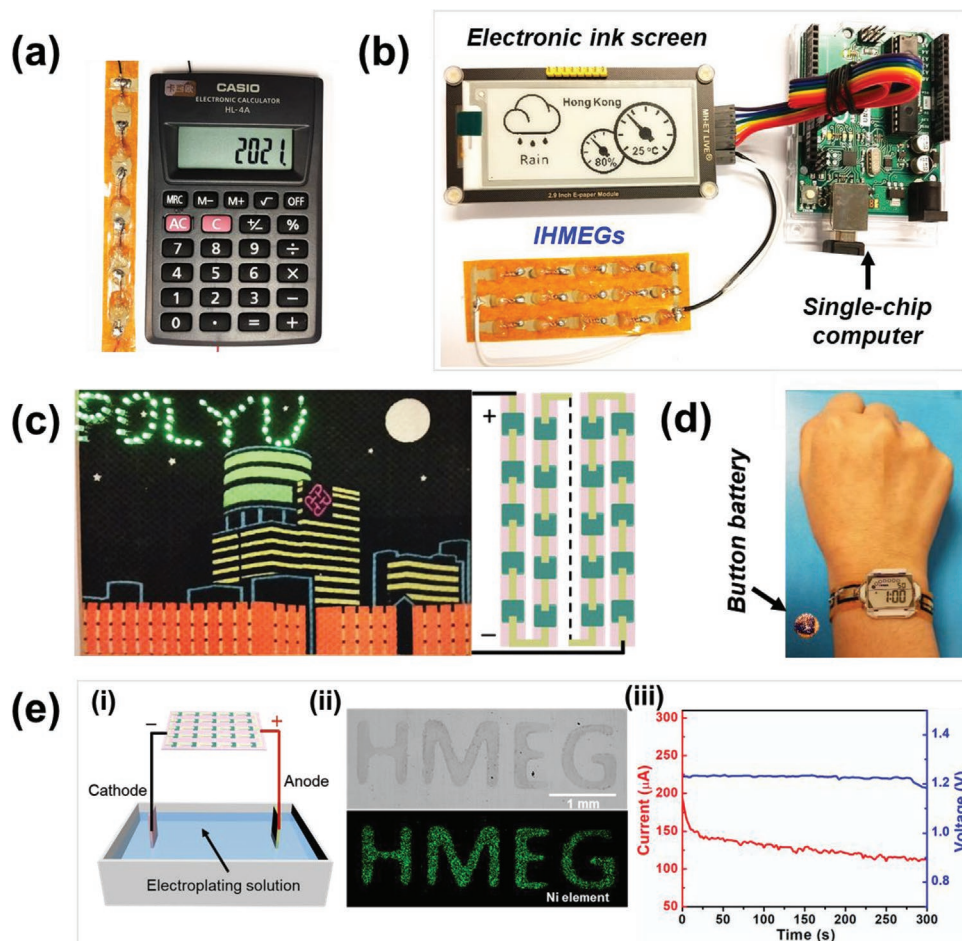


**Figure 6.** The applications of IHMEGs as a direct power source. a) Demonstration of  $1 \times 5$  serial IHMEG package as a power-supplying source for directly driving an electronic calculator. b) Schematic of the circuit design and working demonstration of the self-powered electronic ink screen by IHMEG device with  $3 \times 5$  series-parallel connection. The circuit primarily consists of three elements: electronic ink screen, electricity supply using the integrated IHMEG devices, and a single-chip computer to input the display message. c) The serial “POLYU” LEDs directly driven by integrated IHMEGs. d) Wearable demonstration of  $1 \times 5$  serial IHMEG package as energy watchband to power an electronic watch, which normally uses button battery CR2032. e) Electro-deposition of Nickel millimeter-level structure by  $5 \times 5$  IHMEGs device: i) Schematic plot of the setup for the Ni electroplating by using  $5 \times 5$  IHMEGs. ii) SEM image and EDS mapping of the deposited nickel pattern. iii) The work voltage and current between the cathode and anode.

to charge a capacitor to required voltages (Figure 5f) within 100 s directly.

According to different application scenarios, the IHMEG units can be arbitrarily connected in serial or parallel or their combination as required, to drive many kinds of commercial electronics without any additional rectifying circuits and capacitors. For instance, as depicted in Figure 6c, an electronic calculator can be easily powered by only 5 IHMEG units, and a IHMEG device with  $3 \times 5$  series-parallel connection is even sufficient to directly power a dynamic electronic ink screen with a size of  $9 \times 4.6 \text{ cm}^2$  (Figure 6a; Video S1, Supporting Information). Besides, as shown in Figure 6b and Video S2, Supporting Information, by scalable connection of 260 units, 53 LEDs array can be continuously illuminated, well demonstrating the high electricity output of IHMEG to power different optoelectronics for daily use. More importantly, it is worth noting that the IHMEG is small-sized, lightweight, and flexible, making it especially suitable for wearable electronics. As an example, in Figure 6d, a wearable self-powered watch, was designed and

displayed by employing a five-IHMEG-serial package as the energy watchband. Compared with rigid button battery, the IHMEG watchband is highly flexible to be conformably bent around the wrist with little wearing discomfort, promising the potential application for self-powered wearable electronic system.

For further practical application, our IHMEG power device was successfully employed to electroplate metal nickel (Ni) structures on the millimeter scale. The detailed process is illustrated in Figure S14, Supporting Information. First, the photoresist was coated on the copper (Cu) plate as a mask layer, followed by the standard photolithograph to create the desired pattern on the photoresist. Then, Ni electroplating was implemented with the Cu plate as the cathode and Ni plate as the anode. The final step is to remove the photoresist. The  $5 \times 5$  series parallel IHMEG device was integrated to directly power the electro-deposition process (Figure 6e). The scanning electron microscope (SEM) image and Ni element mapping clearly show that the well-defined Ni pattern is successfully electroplated (Figure 6e-ii; Figure S14b, Supporting Information). The

cross-sectional image reveals the formation of densely packed grain structure of the Ni layer with about 500 nm thickness (Figure S14c, Supporting Information). The work current and voltage between the two electrodes are about 130  $\mu\text{A}$  and 1.2 V during 5 mins' electroplating (Figure 6e–iii), showing a high working power output by a small packed IHMEG. Such flexible and easy-integrated IHMEGs are highly desirable and convenient in practical wearable applications.

### 3. Conclusion

In this work, we have developed a versatile, flexible, light-weight, and adaptable IHMEG comprising ionic hydrogel of PVA, PA with hygroscopic glycerol, which forms asymmetric adsorption on flexible fibrous substrates. Taking advantage of synergistic effect of enhanced moisture-absorbing and accompanying ionic clusters diffusion, one single IHMEG unit generates DC electricity with an  $V_{oc}$  of  $\approx 0.8$  V for over 1000 h and a high short-circuit current density of  $0.24$  mA  $\text{cm}^{-2}$  at 80% RH and room temperature. Connected with a matching external load, the unit provides a maximum power density of  $35$   $\mu\text{W}$   $\text{cm}^{-2}$ . The IHMEG operates stably in a wide range of environmental conditions, from 10% to 85% RH and from  $-24$  to  $60$   $^{\circ}\text{C}$ . In situ FTIR spectroscopy and micro-Raman spectroscopy mapping reveal that the moisture-induced directional movement of mass protons within the hydrogel of IHMEG accelerates the high generation of electric power, and long-maintained water gradient guarantees stable voltage output. Moreover, DC power source devices can be easily designed and fabricated by connecting multiple IHMEG units in serial or parallel fashion or combinations according to operating requirements. A scalable 210 V in serial or 7 mA in parallel IHMEG device exceeds most of scalable MEGs in a DC output mode under the only interaction of moisture in the atmosphere, which are sufficient to drive calculators, electronic watches, a dynamic electronic ink screen, and nickel electro-deposition setup and even light-emitting-diode arrays. Working in wide ranges of humidity and temperature, our IHMEG device shows great potentials to develop high-efficient, scalable, flexible, and versatile power sources for self-powered IoT and wearable electronics systems.

### 4. Experimental Section

**Materials:** PVA (degree of hydrolysis: 99%,  $M_n$ : 100 000) was purchased from Chem Co., Ltd. PA (50 wt% in water) solution and glycerol (99%, extra pure) were offered by Acros Organics, Co., Ltd. The fibrous polyimide (FPI) membrane was kindly provided by Changchun Gao Qi polyimide material Co., Ltd, China. Conductive silver paste was supplied by Sigma Aldrich Co., Ltd. Bromophenol blue indicator 0.1% w/v in isopropyl alcohol was purchased from Aladdin Co., Ltd. All reagents were used without further treatment.

**Preparation of IHMEG Units and Integrated Devices:** First, 10 g water and 8.7 g glycerol were uniformly mixed to prepare a binary solvent. Then 3 g PVA and 5 mL PA (24 wt%) were added into above solvent and dissolved at  $95$   $^{\circ}\text{C}$  for 2 h to achieve a homogeneous solution. The mixed solution was drop-casted onto the FPI membrane with screen-printed Ag electrodes and copper connections. The final thickness and size were regulated by dropped volume over the unit area. Typically, a 250  $\mu\text{L}$  solution dropped onto  $1$   $\text{cm}^2$  area yielded an average film

thickness of about 100  $\mu\text{m}$ . A typical IHMEG device owns the area of  $0.25$   $\text{cm}^2$ . Finally, a copper electrode was placed and adhered on the top of the hydrogel of the IHMEG. As the control devices, IHMEGs of pure PVA, and PVA-PA were prepared by the similar process. The films of PVA, PVA-PA, and PVA-PA-glycerol were drop-casted with 500  $\mu\text{L}$  volume or 200  $\mu\text{m}$  thickness for FTIR, Raman, and KPFM tests.

**Characterization and Measurement:**  $I$ – $V$  characteristics,  $V_{oc}$ ,  $I_{sc}$ , and current with external loads were tested by Keithley 2400 (Tektronix, USA). The RH in the testing chamber was controlled by applying different saturated salt vapor, meanwhile with the RH monitored using a hygrometer (COS-03, Shandong Renke Control Technology Co., Ltd., China). An environmental chamber was employed to regulate the temperature from  $-24$  to  $60$   $^{\circ}\text{C}$  meantime with the RH kept at 80%. All other RH tests were carried out at room temperature unless otherwise stated. For bending tests, the samples had a device size of  $0.25$   $\text{cm}^2$  with the gauge length of 50 mm. Cyclic bending test and compression test were implemented by Instron 5566, with Keithley 2400 recording the voltage change simultaneously at 70% RH. For compression test, the samples with a device size of  $0.25$   $\text{cm}^2$  was compressed by Instron 5566 under a compression load of 3 N.

The chemical structures of samples were characterized by FTIR spectroscopy (Spectrum 100, PerkinElmer, USA) in attenuated total-reflection (ATR) model, with the scanning range of  $650$ – $4000$   $\text{cm}^{-1}$  and resolution of  $4$   $\text{cm}^{-1}$  over 16 scans. To in situ track the water diffusion process, the samples were vacuumed and dried for 2 days first and then scanned by ATR-FTIR every 5 min once they were exposed in the air under 65% RH. For further in-depth analysis of water diffusion process at the molecular level, 2D correlation ATR-FTIR spectra were processed and drawn by 2DCS software, developed by Zhou.<sup>[53]</sup> The linear baseline corrections were processed in the regions of  $3700$ – $3000$   $\text{cm}^{-1}$  first. In 2D correlation FTIR spectra, blue and pink cross peaks in the contour maps denote negative and positive correlation peaks, respectively. Raman spectra were obtained by Renishaw Micro-Raman Spectroscopy System using a green LED laser (532 nm). Similarly, the samples were vacuumed and dried for 2 days first and then scanned every 10 min once they were exposed in the air under 65% RH. KPFM was conducted on a Scanning Probe Microscope (Asylum MFP-3D Infinity). SEM (VEGA3 TESCAN, Czech) and energy dispersive X-ray spectroscopy (EDS) were employed to study the deposited "IHMEG" pattern and element analysis.

**Statistical Analysis:** The statistical analysis was conducted by using Excel 2013 software. The sample size ( $n$ ) for each statistical analysis was given in each figure legend. Relevant data were raw and expressed as mean  $\pm$  standard deviation (SD).

### Supporting Information

Supporting Information is available from the Wiley Online Library or from the author.

### Acknowledgements

This research was partially supported by the Research Grants Council of Hong Kong, China (No.15200917E, 15201419E, and 15202020E), Innovation and Technology Commission (No. ITS/306/17), Endowed Professorship Fund, The Hong Kong Polytechnic University (No.847A), and postgraduate scholarships by the Hong Kong Polytechnic University. The authors thank the technicians Vincent Tang, C. W. Lee, Y. C. Tam from Industrial Center of Hong Kong Polytechnic University for the technical support on electro-deposition.

### Conflict of Interest

The authors declare no conflict of interest.

## Data Availability Statement

The data that support the findings of this study are available in the Supporting Information of this article.

## Keywords

direct-current electricity, ionic hydrogels, moisture, wearable electronics

Received: January 21, 2022

Revised: March 21, 2022

Published online:

- [1] X. Liu, H. Gao, J. E. Ward, X. Liu, B. Yin, T. Fu, J. Chen, D. R. Lovley, J. Yao, *Nature* **2020**, 578, 550.
- [2] W. Xu, H. Zheng, Y. Liu, X. Zhou, C. Zhang, Y. Song, X. Deng, M. Leung, Z. Yang, R. X. Xu, *Nature* **2020**, 578, 392.
- [3] Z. Zhang, X. Li, J. Yin, Y. Xu, W. Fei, M. Xue, Q. Wang, J. Zhou, W. Guo, *Nat. Nanotechnol.* **2018**, 13, 1109.
- [4] M. Li, M. Hong, M. Dargusch, J. Zou, Z.-G. Chen, *Trends Chem.* **2021**, 3, 561.
- [5] C.-G. Han, X. Qian, Q. Li, B. Deng, Y. Zhu, Z. Han, W. Zhang, W. Wang, S.-P. Feng, G. Chen, *Science* **2020**, 368, 1091.
- [6] D. Zhao, H. Wang, Z. U. Khan, J. Chen, R. Gabrielsson, M. P. Jonsson, M. Berggren, X. Crispin, *Energy Environ. Sci.* **2016**, 9, 1450.
- [7] J. Bai, Y. Huang, H. Cheng, L. Qu, *Nanoscale* **2019**, 11, 23083.
- [8] H. Cheng, Y. Huang, F. Zhao, C. Yang, P. Zhang, L. Jiang, G. Shi, L. Qu, *Energy Environ. Sci.* **2018**, 11, 2839.
- [9] H. Wang, Y. Sun, T. He, Y. Huang, H. Cheng, C. Li, D. Xie, P. Yang, Y. Zhang, L. Qu, *Nat. Nanotechnol.* **2021**, 16, 811.
- [10] D. Shen, W. W. Duley, P. Peng, M. Xiao, J. Feng, L. Liu, G. Zou, Y. N. Zhou, *Adv. Mater.* **2020**, 32, 2003722.
- [11] L. Li, Z. Chen, M. Hao, S. Wang, F. Sun, Z. Zhao, T. Zhang, *Nano Lett.* **2019**, 19, 5544.
- [12] Y. Huang, H. Cheng, L. Qu, *ACS Mater. Lett.* **2021**, 3, 193.
- [13] T. Xu, X. Ding, Y. Huang, C. Shao, L. Song, X. Gao, Z. Zhang, L. Qu, *Energy Environ. Sci.* **2019**, 12, 972.
- [14] K. S. Moreira, D. Lermen, L. P. dosSantos, F. Galembeck, T. A. Burgo, *Energy Environ. Sci.* **2021**, 14, 353.
- [15] Y. Liang, F. Zhao, Z. Cheng, Y. Deng, Y. Xiao, H. Cheng, P. Zhang, Y. Huang, H. Shao, L. Qu, *Energy Environ. Sci.* **2018**, 11, 1730.
- [16] J. Xue, F. Zhao, C. Hu, Y. Zhao, H. Luo, L. Dai, L. Qu, *Adv. Funct. Mater.* **2016**, 26, 8784.
- [17] M. Li, L. Zong, W. Yang, X. Li, J. You, X. Wu, Z. Li, C. Li, *Adv. Funct. Mater.* **2019**, 29, 1901798.
- [18] Y. Huang, H. Cheng, C. Yang, P. Zhang, Q. Liao, H. Yao, G. Shi, L. Qu, *Nat. Commun.* **2018**, 9, 4166.
- [19] J. Bai, Y. Huang, H. Wang, T. Guang, Q. Liao, H. Cheng, S. Deng, Q. Li, Z. Shuai, L. Qu, *Adv. Mater.* **2021**, 34, 2103897.
- [20] Y. Huang, H. Cheng, C. Yang, H. Yao, C. Li, L. Qu, *Energy Environ. Sci.* **2019**, 12, 1848.
- [21] S. Zheng, J. Tang, D. Lv, M. Wang, X. Yang, C. Hou, B. Yi, G. Lu, R. Hao, M. Wang, Y. Wang, H. He, X. Yao, *Adv. Mater.* **2021**, 34, 2106410.
- [22] F. Zhao, H. Cheng, Z. Zhang, L. Jiang, L. Qu, *Adv. Mater.* **2015**, 27, 4351.
- [23] C. Yang, Y. Huang, H. Cheng, L. Jiang, L. Qu, *Adv. Mater.* **2019**, 31, 1805705.
- [24] D. Shen, M. Xiao, G. Zou, L. Liu, W. W. Duley, Y. N. Zhou, *Adv. Mater.* **2018**, 30, 1705925.
- [25] H. Wang, H. Cheng, Y. Huang, C. Yang, D. Wang, C. Li, L. Qu, *Nano Energy* **2020**, 67, 104238.
- [26] Z. Sun, L. Feng, C. Xiong, X. He, L. Wang, X. Qin, J. Yu, *J. Mater. Chem. A* **2021**, 9, 7085.
- [27] A. Li, Y. Zi, H. Guo, Z. L. Wang, F. M. Fernández, *Nat. Nanotechnol.* **2017**, 12, 481.
- [28] Y. Guo, J. Bae, Z. Fang, P. Li, F. Zhao, G. Yu, *Chem. Rev.* **2020**, 120, 7642.
- [29] F. Ni, N. Qiu, P. Xiao, C. Zhang, Y. Jian, Y. Liang, W. Xie, L. Yan, T. Chen, *Angew. Chem., Int. Ed.* **2020**, 59, 19237.
- [30] Q. Hu, G. Li, X. Liu, B. Zhu, X. Chai, Q. Zhang, J. Liu, C. He, *Angew. Chem.* **2019**, 131, 4362.
- [31] V. R. Feig, H. Tran, M. Lee, Z. Bao, *Nat. Commun.* **2018**, 9, 2740.
- [32] J. Lopez, Y. Sun, D. G. Mackanic, M. Lee, A. M. Foudeh, M. S. Song, Y. Cui, Z. Bao, *Adv. Mater.* **2018**, 30, 1804142.
- [33] Y. Shi, J. Zhang, A. M. Bruck, Y. Zhang, J. Li, E. A. Stach, K. J. Takeuchi, A. C. Marschilok, E. S. Takeuchi, G. Yu, *Adv. Mater.* **2017**, 29, 1603922.
- [34] J. Bae, Y. Li, J. Zhang, X. Zhou, F. Zhao, Y. Shi, J. B. Goodenough, G. Yu, *Angew. Chem., Int. Ed.* **2018**, 57, 2096.
- [35] Y. Shi, L. Peng, G. Yu, *Nanoscale* **2015**, 7, 12796.
- [36] Y. Guo, G. Yu, *Acc. Mater. Res.* **2021**, 2, 374.
- [37] Z. A. Akbar, J.-W. Jeon, S.-Y. Jang, *Energy Environ. Sci.* **2020**, 13, 2915.
- [38] X. Pan, Q. Wang, R. Guo, S. Cao, H. Wu, X. Ouyang, F. Huang, H. Gao, L. Huang, F. Zhang, L. Chen, Y. Ni, K. Liu, *J. Mater. Chem. A* **2020**, 8, 17498.
- [39] F. Zhao, Y. Liang, H. Cheng, L. Jiang, L. Qu, *Energy Environ. Sci.* **2016**, 9, 912.
- [40] K. Liu, P. Yang, S. Li, J. Li, T. Ding, G. Xue, Q. Chen, G. Feng, J. Zhou, *Angew. Chem., Int. Ed.* **2016**, 55, 8003.
- [41] Y. Liang, F. Zhao, Z. Cheng, Y. Deng, Y. Xiao, H. Cheng, P. Zhang, Y. Huang, H. Shao, L. Qu, *Energy Environ. Sci.* **2018**, 11, 1730.
- [42] N. Bonanos, *Solid State Ionics* **2001**, 145, 265.
- [43] X. M. Liu, H. Y. Gao, J. E. Ward, X. R. Liu, B. Yin, T. D. Fu, J. H. Chen, D. R. Lovley, J. Yao, *Nature* **2020**, 578, 550.
- [44] J. Park, S. Song, Y. Yang, S.-H. Kwon, E. Sim, Y. S. Kim, *J. Am. Chem. Soc.* **2017**, 139, 10968.
- [45] H. Jin, S. G. Yoon, W. H. Lee, Y. H. Cho, J. Han, J. Park, Y. S. Kim, *Energy Environ. Sci.* **2020**, 13, 3432.
- [46] G. Xue, Y. Xu, T. Ding, J. Li, J. Yin, W. Fei, Y. Cao, J. Yu, L. Yuan, L. Gong, *Nat. Nanotechnol.* **2017**, 12, 317.
- [47] J. Bae, M. S. Kim, T. Oh, B. L. Suh, T. G. Yun, S. Lee, K. Hur, Y. Gogotsi, C. M. Koo, I.-D. Kim, *Energy Environ. Sci.* **2022**, 15, 123.
- [48] I. Noda, *Appl. Spectrosc.* **1993**, 47, 1329.
- [49] M. Wang, P. Wu, S. S. Sengupta, B. I. Chadhary, J. M. Cogen, B. Li, *Ind. Eng. Chem. Res.* **2011**, 50, 6447.
- [50] C. Sammon, J. Yarwood, N. Everall, *Polymer* **2000**, 41, 2521.
- [51] M. Liu, P. Wu, Y. Ding, G. Chen, S. Li, *Macromolecules* **2002**, 35, 5500.
- [52] J.-W. Shin, N. Hammer, E. Diken, M. Johnson, R. Walters, T. Jaeger, M. Duncan, R. Christie, K. D. Jordan, *Science* **2004**, 304, 1137.
- [53] T. Zhou, A. Zhang, C. Zhao, H. Liang, Z. Wu, J. Xia, *Macromolecules* **2007**, 40, 9009.